Spin-orbit coupling induced robust spin-Seebeck effect and pure thermal spin currents in achiral molecule systems

Hua-Hua Fu, Gui-Fang Du, Dan-Dan Wu, Qing-Bo Liu, and Ruqian Wu

Phys. Rev. B **100**, 085407 — Published 7 August 2019

DOI: 10.1103/PhysRevB.100.085407

Spin-orbit coupling induced robust spin-Seebeck effect and pure thermal spin currents in achiral molecule systems

Hua-Hua Fu[1,2,*] Gui-Fang Du[1], Dan-Dan Wu[1], Qing-Bo Liu[1], and Ruqian Wu[2,†]
[1]*School of Physics and Wuhan National High Magnetic field center, Huazhong University of Science and Technology, Wuhan 430074, People's Republic of China.*
[2]*Department of Physics and Astronomy, University of California, Irvine, California 92697-4575, United States.*
(Dated: July 8, 2019)

Spin-Seebeck effect (SSE) is an effective route to realize pure spin current by using spin-polarized electrons or spin-wave transport in magnetic systems. Here we propose a new route, i.e., by using spin-orbit coupling (SOC), to achieve robust SSE characterized by pure thermal spin current. The material examples are constructed on achiral nanotubes, and the theoretical results reveal that: (i) as temperature gradient is applied along the nanotubes, thermal spin-up and spin-down currents with opposite flow directions are produced without any accompanying charge current; (ii) the SSE is robust against decoherence and non-uniform interchain SOC; (iii) the thermal spin currents display a multi-oscillation feature with increasing device temperatures, supporting their potential device applications in thermal spin-current multi-switcher; and (vi) strain engineering in the radical direction of nanotubes is an effective way to improve SSE and to control pure thermal spin current. These inspiring spin transport behaviors in achiral molecular systems put forwards a new mechanism to realize the robust SSE characterized by pure spin current, and develop the research field of spin-orbito-caloritronics which focuses on the interplay of electrons' spin and orbital degrees of freedom in the presence of temperature gradient.

PACS number(s): 73.63.-b, 73.23.Hk, 75.47.-m, 75.75.-c

I. INTRODUCTION

Spin caloritronics, one of a rapidly developing research fields in spintronics, is devoted to using the excess heat generated in nanoscale materials and devices to drive spin current[1,2]. The core topic in this field is the spin-Seebeck effect (SSE), which has long been regarded as a feasible way to achieve pure spin current by the thermal gradient in magnetic insulators[3–6]. To push SSE towards practical device applications, it is desired to suppress thermally driven charge current, because it causes energy dissipation due to the Joule law. To the end, we usually adopt two kinds of spin currents generated by SSE. One is the thermally driven spin-wave current that has no accompanying charge flow, since the angular momentum is carried by spin wave or magnon propagation in magnetic insulators[7–10]. The other one is the thermally driven spin-dependent currents, in which the conduction electrons having different spins flow in opposite directions[11–15]. For the latter case, we have suggested to generate the thermal spin-up and spin-down currents along edges of ferromagnetic nanoribbons[11,12]. Nevertheless, the edge-related spin transport may reduce the overlap of the spin transport channels in space, which is not favorable for the cancellation of charge current. Moreover, the edge magnetism in nanoribbons or other nanoscale systems can be weakened easily by increasing temperature. In addition, a large temperature gradient in low-dimensional systems may decrease the thermal stability of materials. These drawbacks inspire us to explore new mechanisms and materials for realization of SSE and pure thermal spin current with conducting electrons[16,17].

More recently, an important finding in spintronics is that DNA molecules can serve as efficient spin filters[18,19], due to the chiral-induced spin selectivity effect (CISS). This effect has attracted increasing attention, because it not only paves the way to a novel paradigm of spin injection at chiral/semiconductor interfaces[20], but also offers a new possibility to design spintronic devices, such as spin filter on the basis of nonmagnetic or organic materials[21]. Furthermore, through measuring the magnetoresistance effect, the CISS-induced spin filtering was confirmed in helicene molecules adsorbed as an oriented monolayer on an oriented pyrolytic graphite substrate[22]. Apart from these, a tunable spin switching behavior and the thermopower with an on-off ratio of several orders of magnitude combined with high thermoelectric figure-of-merit were found in a helicene molecule through controlling the length of the helicene molecule[23]. Naturally, a question arises here: can this kind of molecular systems generate pure thermal spin current and other unusual spin transport behaviors as desired for new spintronic materials?

Meanwhile, to understand the underlying physical mechanism of CISS, a theoretical model has been put forwards to interpret spin-resolved transport through ds-DNA and the α-helical protein[24–26]. Theoretical studies revealed that two key factors, i.e., spin-orbit coupling (SOC) and intrinsic chiral structure, cause the high spin filtration efficiency in the helicene molecules. However, it should be stressed that a recent theoretical work found that the emergence of CISS and the spin-splitting transport can also occur in an achiral and nonmagnetic nanotubes, and uncovered that the helical symmetry may not be necessary for the emergence of CISS, while the SOC is required even though its magnitude can be weak[27]. Moreover, the key role of SOC on the spin-slitting effect in a double helix emulating DNA chain has also been

analysed[28]. As a further step beyond these studies, we constructed an achiral nanotube [see Fig. 1(a)] to explore the SOC-induced SSE and the generation of pure thermal spin current in low-dimensional quantum systems. Our theoretical results show that if we produce a temperature gradient between two nonmagnetic metal leads, the spin-up and spin-down currents with the opposite flow directions are generated with equal magnitudes through the nanotube in the presence of the SOC, supporting that a perfect SSE without any accompanying charge current occurs here. Moreover, the SSE is robust against decoherence and non-uniform interchain SOCs. The thermally induced spin currents display a multi-oscillation feature with increasing device temperatures, indicating its potential applications in pure-spin-current multi-switcher. In addition, the strain engineering in the radical direction of nanotubes is an effective approach to control and improve the SSE. These results indicate that the SOC can be an effective mechanism to realize the robust SSE to produce pure spin currents. Two separate research fields viz. spin caloritronics[1,2] and spin orbitronics[29,30] may hence converge together to a new research subject, i.e., spin-orbito-caloritronics.

The remainder of this paper is organized as follows. In Sec. II, we construct an achiral nanotube with two thermal nonmagnetic leads at different temperatures, and we propose a model Hamiltonian to describe the electron hopping and decoherence under the influence of the SOC. In Sec. III, the thermally driven spin-up and spin-down currents are numerically calculated, the spin transport behavior of the nanotube is discussed, and an effective route to improve and control the SSE is proposed. Finally, the key results are summarized in Sec. IV.

II. DEVICE MODELS AND THEORETICAL METHOD

In Fig. 1(a), a thermal spin device composed of an achiral nanotube coupled with two nonmagnetic thermal leads with different temperatures is proposed. The related model Hamiltonian is described by the following one:

$$H = H_{mol} + H_{so} + H_d + H_{lead}, \tag{1}$$

where the Hamiltonian $H_{mol} = \hat{\mathbf{p}}^2/2m + V$ describes the kinetic and potential energies of the electrons in the nanotube, with $\hat{\mathbf{p}}$ being the electron momentum operator and m being the electron effective mass. The second term, $H_{so} = (\hbar/4m^2c^2)\nabla V \cdot (\hat{\sigma} \times \hat{\mathbf{p}})$ is the SOC Hamiltonian, where $\hbar$ is the reduced Plank constant, c is the speed of light, and $\hat{\sigma} = (\sigma_x, \sigma_y, \sigma_z)$ is a vector in spin space whose components are the three Pauli matrices $\sigma_{x,y,z}$.

In what follows, we discretize H_{mol} and H_{so} on the basis set constructed by the nanotube lattices with the amplitude of the electron wave function being $\psi_{j,n}$ at site $\{j,n\}$ as similar at the procedure adopted in Ref. [31]. Then, the discretized form of H_{mol} is

$$H_{mol} = \sum_{j=1}^{J}[\sum_{n=1}^{N} \varepsilon_{jn} c_{jn}^{\dagger} c_{jn} + \sum_{n=1}^{N-1} t_{\parallel} c_{jn}^{\dagger} c_{j,n+1} + \sum_{n=1}^{N} t_{\perp} c_{jn}^{\dagger} c_{j+1,n} + \text{H.c.}], \tag{2}$$

where $c_{J+1,n}^{\dagger} \equiv c_{1n}^{\dagger}$ and $c_{jn}^{\dagger} = (c_{jn\uparrow}^{\dagger}, c_{jn\downarrow}^{\dagger})$ is the creation operator at the site $\{j,n\}$ of the nanotube, J is the number of the chains, N is the length of nanotube, and the index $\{j,n\}$ indicates the site n of the chain j. $\varepsilon_{jn} = \langle\psi_{j,n}|H_{mol}|\psi_{j,n}\rangle$ is the potential energy, $t_{\parallel} = \langle\psi_{j,n}|H_{mol}|\psi_{j,n+1}\rangle$ is the intrachain hopping integral, and $t_{\perp} = \langle\psi_{j,n}|H_{mol}|\psi_{j+1,n}\rangle$ is interchain hopping integral, since the nearest-neighbour (NN) hopping is considered in the nanotube. It is noted that the wave function $\psi_{j,n}$ decays exponentially with the distance in the potential barrier, i.e., $\psi_{j,n}(l) \sim e^{l/l_c}$, where l is the distance from site $\{j,n\}$, and l_c is the decay exponent. Similarly, by calculating $\langle\psi_{j,n}|H_{so}|\psi_{j+1,n}\rangle$ and $\langle\psi_{j,n}|H_{so}|\psi_{j,n+1}\rangle$, the SOC Hamiltonian is written as

$$H_{so} = \sum_{j=1}^{J}[2i\sum_{n=1}^{N-1} c_{jn}^{\dagger} s_{jn} \sigma_j c_{j,n+1} + 2i\sum_{n=1}^{N} c_{jn}^{\dagger} \omega_{jn} \sigma_z c_{j+1,n} + \text{H.c.}]. \tag{3}$$

Here, $s_{jn} = s\ e^{-(l_{jn,j(n+1)}-l)/l_c}$ is the intrachain SOC strength between two sites $\{j,n\}$ and $\{j,(n+1)\}$, where the SOC strength is s when the distance is l; ω_{jn} is the interchain SOC strength between the sites $\{j,n\}$ and $\{(j+1),n\}$, and can be reduced to $\omega = s\ cos(\Delta\phi/2)$ when the NN approximation is considered; $\sigma_j = \sigma_x \sin\phi_j - \sigma_y \cos\phi_j$, $\phi_j = (j-1)\Delta\phi$, with $\Delta\phi = 2\pi/J$.

The third term of the Hamiltonian, H_d, denotes the phase-breaking processes, which can be imitated by connecting each site of the molecule to one of Büttiker virtual leads. In the frame of tight-binding model, H_d is expressed as the following form

$$H_d = \sum_{j,n,k} (\varepsilon_{jnk} d_{jnk}^{\dagger} d_{jnk} + t_d d_{jnk}^{\dagger} c_{jn} + \text{H.c.}), \tag{4}$$

where $d_{jnk}^{\dagger} = (d_{jnk\uparrow}^{\dagger}, d_{jnk\downarrow}^{\dagger})$ denotes the creation operator of the mode k in Büttiker virtual leads, and t_d is the coupling between the nanotube and the virtual lead with the strength Γ_d[24,25,32]. During the charge transport process, an electron may suffer inelastic scatterings from, e.g., phonons, unclear spins, and impurities, which leading to the loss of phase memory of the electron[27].

The Hamiltonian $H_{lead} = \sum_k [\varepsilon_k (a_{Lk}^{\dagger} a_{Lk} + a_{Rk}^{\dagger} a_{Rk}) + \tau(a_{Lk}^{\dagger} c_{11} + a_{Rk}^{\dagger} c_{jN} + \text{H.c.})]$ describes the two nonmagnectic metallic leads, and their coupling to the nanotube. The first two terms are the Hamiltonian of two leads with different temperatures, and the last two terms describe

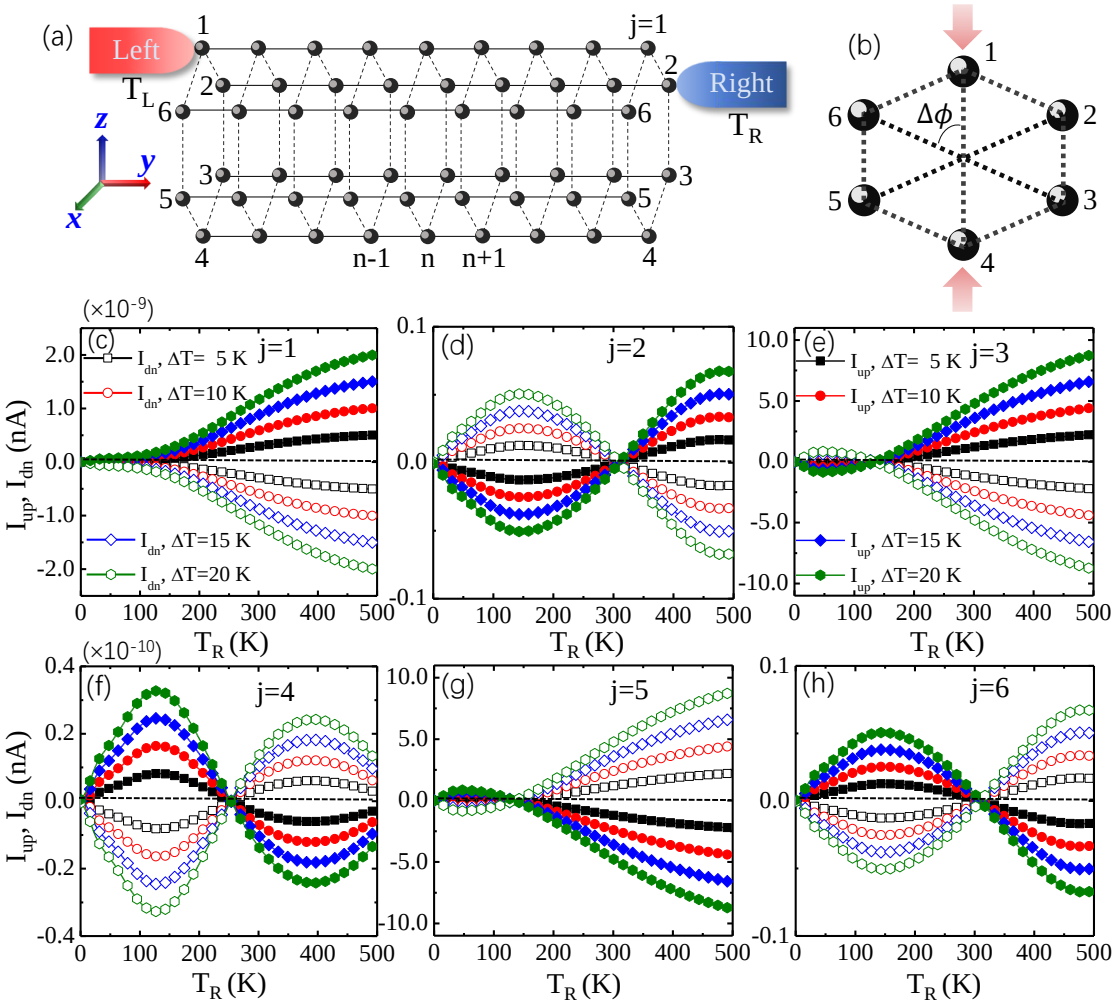

FIG. 1. (a) Schematic view of an achiral nanotube (no helical symmetry) whose site {1,1} and {2,N} are coupled to left and right nonmagnetic leads with the temperature T_L and T_R, respectively. (b) A compression strain engineering is applied to adjust the SOCs in nanotubes. (c)-(h) The thermal spin-up current I_{up} and spin-down one I_{dn} versus T_R, where the temperature gradient ΔT ($= T_L - T_R$) is set as 5, 10, 15 and 20 K. The index $\{j,\ n\}$ denotes site n of chain j, the number of chains is $J = 6$, the SOC strength is $s = 0.05$, the coupling to Büttiker's virtual leads is $\Gamma_d = 0.04$ and the nanotube length is $N = 20$.

the coupling between the two leads and the nanotube with the strength τ. It should be noted that $a^\dagger_{Lk}(a^\dagger_{Rk})$ is the creation operator for an electron in the left (right) lead. In the device design, we consider that the left lead is always coupled to the site {1,1}, and the right lead is coupled to the site $\{j, N\}$, while the site index j is chosen in the last ring as shown in Fig. 1(a).

In the Landauer-Büttiker formulism, the spin-dependent currents are given by the following equation[33]

$$I_\sigma = \frac{e}{h}\int Tr[\mathrm{T}^\sigma(E)(F_L(E,\mu_L,T_L) - F_R(E,\mu_R,T_R))]dE, \tag{5}$$

where e is the electron charge, h is the Planck's constant, and $\sigma = \uparrow$ or $\downarrow$ indicates the spin index. $F_{L(R)} = \{1 + \exp[(E - \mu_{L(R)})/k_B T_{L(R)}]\}^{-1}$ is the Fermi distribution function of the left (right) lead with temperature $T_{L(R)}$ and chemical potential $\mu_{L(R)}$. The spin-dependent transmission coefficient of the nanotube $\mathrm{T}^\sigma(E)$ can be calculated by using the non-equilibrium Green's function theory in the linear-resonance regime as[34–37]

$$\mathrm{T}^\sigma(E) = \mathrm{Tr}[\Gamma_L G^R(E)\Gamma_R G^A(E)]^\sigma, \tag{6}$$

where $\Gamma_{L/R} = i[\Sigma_{L/R} - \Sigma^\dagger_{L/R}]$ denotes the electron coupling between the nanotube and the left (right) lead with $\Sigma_{L/R}$ being the related self-energy term. $G^{R/A}(E)$ indicates the retarded (advanced) Green's function of the central region, $G^R(E) = [H_{cen} - (E + i\eta) + \Sigma_L + \Sigma_R]$ and $G^A(E) = [G^R(E)]^\dagger$, where $H_{cen} = H_{mol} + H_{so} + H_d$. In our numerical calculations, the electron hoping integrals $t_\perp = t_\parallel = t$, and the coupling $\Gamma_{L/R}$ is taken as the energy unit with $\Gamma_{L/R} = t = 1$. The nanotube potential energy is chosen to be $\varepsilon_{jn} = 0$ without loss of generality. In this work, we mainly focus on the spin-dependent currets driven by the temperature gradient ΔT between

two leads, without the presence of any external bias and back voltage.

III. RESULTS AND DISCUSSION

Firstly, to explore the occurrence of SSE in the achiral nanotubes, we chose the size of the achiral nanotube as $j = 6$ and $N = 20$, and set the SOC strength as $s = 0.05$. In the device design, the site $\{1, 1\}$ in the nanotube is contacted to the left lead and the site $\{j, 20\}$ is contacted to the right one, as shown in Fig. 1(a). To illustrate the influence of the spatial symmetry of two thermal terminals on the thermal spin-dependent currents, the site index j runs over all sites in the right ring to construct six different device models, and for convenience, we use the j value to denote the related device. When a temperature gradient ΔT ($=T_L - T_R$) is applied between two leads, the spin-up current I_{up} and spin-down current I_{dn} are generated in the all device configurations as plotted at Figs. 1(c)∼1(h), where ΔT is set from 5 to 20 K. It is inspiring that in all cases, I_{up} and I_{dn} have opposite signs, indicating that they flow in the opposite directions, which supports the occurrence of the SSE based on conducting electrons in this achiral nanotube[11–13]. Since there is no any magnetic impurity or external magnetic fields adopted in the systems, the SSE is induced by the SOC in the achiral nanotube. Moreover, from the thermal spin transport behaviors, the SSE obtained here has several important and unusual features, even some of them have not been found in any magnetic nanoribbons[11,38,39], nanotubes[12,39] or molecular junctions[40] so far.

(i) The curves of I_{up} and I_{dn} versus T_R are exactly symmetric about the zero-current axis in all device configurations, indicating that the charge current I_c ($= I_{up} + I_{dn}$) is exactly suppressed to zero and hence a completely pure spin current I_s ($= \frac{h}{2e}(I_{up} - I_{dn})$) is produced. Thus, a perfect SSE without any accompanying charge current is achieved here.

(ii) The thermally induced spin-dependent currents display an oscillation feature with the increase of T_R apart from the device for $j = 1$ [see Fig. 1(c)]. For example, in the device for $j = 2$, the magnitudes of I_{up} and I_{dn} increase firstly and then decreases symmetrically with T_R. As T_R increases to a critical temperature T_c (≈ 300 K), I_{up} and I_{dn} are equal to zero and then change their flow directions. The appearance of T_c supports that the achiral nanotube can be developed as a thermal spin switcher.

(iii) In both devices with $j = 2$ and 6, or $j = 3$ and 5, the thermal spin transport behaviors are exactly the same, apart from the opposite spin directions in the spin-dependent currents, i.e., $(I_{up})_{j=2(3)} = -(I_{dn})_{j=6(5)}$. This characteristics is attributed to the mirror symmetry in achiral nanotubes.

(iv) The magnitudes of spin-dependent currents are tightly dependent on the sites contacted with the leads. The spin currents flowing through the nanotube devices

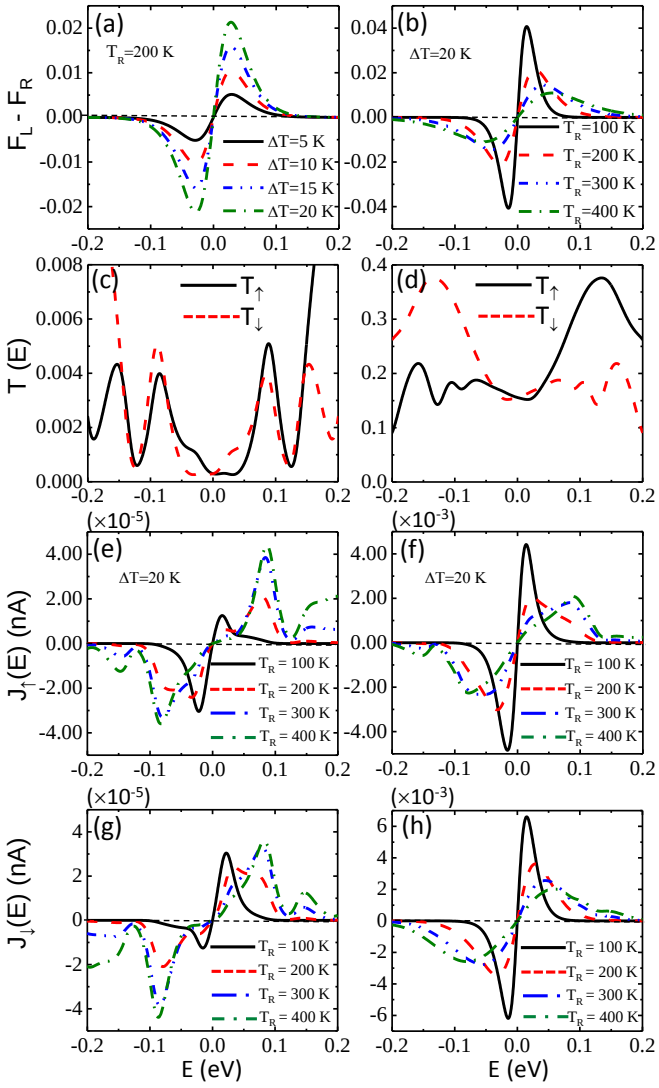

FIG. 2. (a) and (b) The Fermi function difference $F_L - F_R$ between two thermal leads. (c) and (d) Transmission coefficients for spin-up electrons ($T_\uparrow$) and spin-down ones ($T_\downarrow$) as a function of the Fermi energy E in the nanotube devices for $j = 2$ and 3. (e) and (f) Spin current spectra $J_\uparrow(E)$ versus E at various values of T_R and $\Delta T = 20$ K in the devices for $j = 2$ and 3, respectively. (g) and (h) The related spin down spectra $J_\downarrow(E)$ versus E in the above two nanotube devices.

for $j = 3$ and $j = 5$ are much larger than those in other devices, while the thermal spin currents in devices for $j = 1$ and 4 are nearly equal to zero, indicating that the breaking of the mirror symmetry of two thermal leads enhances largely the thermal spin currents.

To understand the occurrence of the perfect SSE with particular spin transport characteristics, we first consider the electron distribution in the leads. Considering that both leads are constructed by the same metal material and possess the same density of state, the Fermi distribution $F_L(T_L) - F_R(T_R)$ determines the difference in carrier concentrations between them. When a

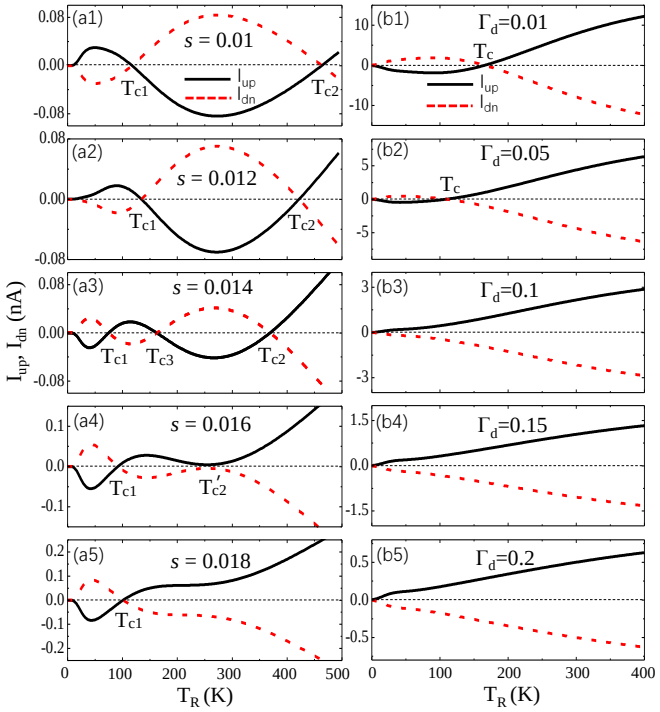

FIG. 3. (a1)-(a5) The thermal spin-up current I_{up} (black lines) and the spin-down one I_{dn} (red dash lines) versus the temperature T_R in the achiral nanotube device for $j = 3$ and $\Delta T = 20$ K, where the SOC strength s is increased from 0.01 to 0.018. (b1)-(b5) I_{up} and I_{dn} versus T_R at $\Delta T = 20$ K in the nanotube device with $j = 3$ and $s = 0.01$, where the decoherence strength Γ_d is increased from 0.01 to 0.2.

temperature gradient ΔT is applied between two leads, $F_L(T_R+\Delta T)-F_R(T_R)$ is longer equal to zero and shows an inverse symmetric behavior about the Fermi level, as shown in Figs. 2(a) and 2(b). Since $F_L - F_R$ is an odd function, the sign of I_σ is determined by the slope of the transmission coefficient T_σ according to Eq. (4)[12,42]. In Figs. 2(c) and 2(d), we plot the spin-dependent transmission $\mathrm{T}_{\uparrow(\downarrow)}$ versus Fermi energy in the nanotube devices for $j = 2$ and 3, respectively. One can find that: (i) the electron-hole symmetries in the spin-up and spin-down electrons are both broken around the Fermi level (-0.1 eV $< E <$ 0.1 eV), resulting in thermally induced spin-up and spin-down currents; (ii) the transmission $\mathrm{T}_{\uparrow(\downarrow)}$ in the device for $j = 3$ is much larger than that in the device for $j = 2$, which supports that the breaking of the mirror symmetry of two leads enhances largely the carrier transport; (iii) the weak breaking of the electron-hole symmetry around the Fermi level leads to the competing transport of the thermally driven electrons and holes, resulting in the changing of the flow directions of the thermal spin-dependent currents at the critical temperature T_c. Moreover, both curves of $\mathrm{T}_\uparrow - E$ and $\mathrm{T}_\downarrow - E$ are symmetric with respect to the line of $E = 0$, i.e., $\mathrm{T}_\sigma(E) = \mathrm{T}_\sigma(-E)$, resulting in the equal spin-up and spin-down currents. These conclusions can be confirmed further by the related spin-dependent current spectra $J_{\uparrow(\downarrow)}(E)(= \mathrm{T}_{\uparrow(\downarrow)}(E)(F_L(E,T_L) - F_R(E,T_R)))$ as drawn in Figs. 2(e)∼2(h). For example, in the nanotube device for $j = 2$, the spin current spectrum $J_{\uparrow(\downarrow)}(E)$ at low T_R is strongly asymmetric in the region -0.1 eV $< E <$ 0.1 eV, resulting in a remarkable net thermal spin-up or spin-down current. While at the temperature $T_R = 300$ K, the related spin-current spectra are nearly symmetric about $E = 0$, resulting in the zero-current points in I_{up} and I_{dn}, regardless of the different values of ΔT.

As one of the conclusions obtained above, the spin-splitting in the achiral nanotubes is induced by the SOC, rather than by magnetic impurities or external magnetic field. To explore this unusual transport behavior of achiral molecule systems, we turn to study the influence of the SOC strength on the thermally driven spin-dependent currents. In Fig. 3, we plot I_{up} and I_{dn} versus T_R in the nanotube device for $j = 3$, in which the SOC strength s is enhanced from 0.01 to 0.018, and ΔT is set as 20 K. It is inspiring that the thermally driven spin-dependent currets display as an oscillation feature with increasing T_R. For example, in the nanotube device with $s = 0.01$, the thermal spin-dependent currents have two zero-current points identified by the critical temperatures T_{c1} and T_{c2} as shown in Fig. 3(a1). Crossing over these two temperatures, both I_{up} and I_{dn} change their flow directions at the same time. As s increases, T_{c2} is driven to low-temperature region, and another critical temperature, i.e., T_{c3}, appears in the curves of spin-up and spin-down currents [see Fig. 3(a3)]. As a result, the thermally driven spin-dependent currents show multi-oscillation behaviors. Apart from these, as s is chosen as a suitable value, T_{c2} may change to the critical temperature related to another kind of zero-current point, where the thermal spin-up and spin-down currents remain their flow directions as they cross over the zero values, as shown in Fig. 3(a4). These intriguing features of thermal spin transports in the SSE induced by SOC have not been found in any magnetic materials, since they are tightly related with the SOC-induced spin-flipping process. In addition, multiple zero-current points appearing in the thermal spin currents support that the present achiral molecule systems have potential for device applications such as multi-switcher of thermal pure spin current.

Since the achiral nanotube works at finite temperatures and the carriers in the related devices are driven by the temperature gradient, electron-phonon coupling or onsite energy disorder exists inevitably, which will give rise to various decoherence phenomena in thermal spin-dependent transport[24,25]. To demonstrate robustness of the SSE and the pure thermal spin currents obtained in the achiral nanotubes, we then study the thermally induced spin-dependent currents by considering the various decoherence strength in the example nanotube device for $j = 3$ with $s = 0.01$. To simulate the lose of electron coherence memory in the inelastic-scattering process, each site in the nanotube is contacted by a Büttiker virtual lead in the numerical calculations[40]. When the decoherence process is introduced into the nanotube and as

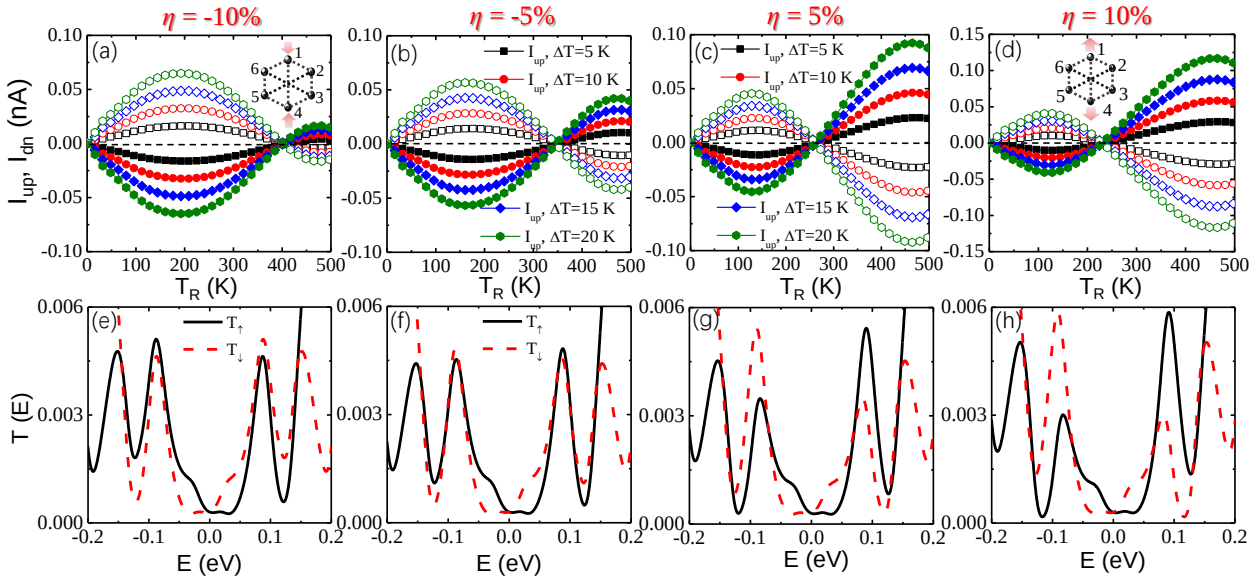

FIG. 4. Strain engineering is applied in the transverse direction of the achiral nanotube device for $j = 2$ with $s = 0.2$ to adjust and improve the SSE and the thermal spin currents. (a)-(d) I_{up} and I_{dn} versus T_R under the different values of ΔT, where the value of the strain proportion is set as $\pm 5\%$ and $\pm 10\%$, respectively. (e)-(f) The spin-dependent transmission spectra of the above four cases versus the Fermi energy.

its strength Γ_d is enhanced, we find that both thermally induced spin-up and spin-down currents are suppressed as shown in the right panel of Fig. 3. Meanwhile, the critical temperature T_c is driven to lower temperatures, even disappears from the spin currents, indicating that the change of flow directions of thermal carriers is influenced remarkably by the decoherence. However, it is exciting that the thermal spin-up and spin-down currents maintain the opposite flowing directions with equal magnitudes, indicating that the perfect SSE with zero charge current obtained here is strongly robust against the decoherence process.

Considering that the interchain SOC parameter ω_{jn} in the achiral nanotube is tightly dependent on the azimuth ϕ_j of site $\{j, n\}$ in the cylindrical coordinate system as illustrated in Fig. 1(b), we believe that the strain engineering in the radical direction of the achiral nanotubes is an effective way to control and improve the SSE in the current systems[43,44]. In fact, nanotubes typically have usually large Yong's modulus in their axial direction while remarkably soft in radical direction[17,45–47]. Here we take the achiral nanotube device for $j = 2$ as an example and the strain engineering is applied in the chains with $j = 1$ and 4, i.e., the z direction shown in Fig. 1(a). When the strain is applied, the interchain SOC parameters are longer uniform and should be expressed as $\omega_{j,j+1}$. For convenience, we set the strain ratio as η, thus $\omega_{1,2} = \omega_{3,4} = \omega_{4,5} = \omega_{6,1} = s\ \cos(\varphi)$ and $\omega_{2,3} = \omega_{5,6} = s\ \cos((\pi - 2\varphi)/2)$, where $\varphi = (1 \pm \eta)\Delta\phi$, and $\eta > 0$ (< 0) indicates the stretching (compression) strain engineering. In Fig. 4, we plotted the numerical results for thermally induced spin-dependent currents in the achiral nanotube device, where η is changed from -10% to 10%. At the first glance, the spin-up and spin-down currents maintain the high symmetry about the zero-current axis, regardless of the strain engineering strength. Obviously, the the non-uniformness of the interchain SOC don't destroy the SSE, confirming further the robustness of the SOC-induced SSE and the pure thermal spin currents. Furthermore, the magnitudes of the spin-up and spin-down currents together with the critical temperature T_c can be adjusted and controlled easily by the strain engineering. The compression strain engineering increases the electron-hole asymmetry in low-energy region while decreases this symmetry in high-energy region. The stretching strain engineering leads to an opposite results [see Figs. 4(e)∼4(h)].

Interesting, our numerical calculations show that when the strain engineering is applied along the chains with $j = 3$ and 6 in nanotube device, the thermal spin-dependent currents are nearly not influenced (see the Fig. S1 in Supplemental Material [48]). In fact, in the present nanotube device, the two chains applied by the strain have the same symmetry axis as that of two leads. As a result, the mirror symmetry of two leads isn't broken by the strain engineering and the thermal spin-dependent currents are nearly unchanged, which is much different from the former device. Thus we believe that the strain engineering is an effective route to improve and control the SSE and the pure thermal spin currents induced by the SOC in achiral molecule systems, while breaking the mirror symmetry of two leads should be taken into account for this perpose.

IV. CONCLUSION

In summary, we have proposed a new physical mechanism to realize robust SSE in achiral molecule systems. In our proposal, the SSE is induced by the SOC, not by magnetic impurities or external magnetic field. Although the SSE results from thermally driven conduction electrons, there is no any thermal charge current. This perfect SSE with the pure spin currents is strongly robust against the non-uniform interchain SOCs and the decoherence process from inelastic-scattering events. With suitable SOC parameters, the thermally induced spin-up and spin-down currents display multiple oscillation features, indicating that the thermal spin currents can change their flow directions many times, and possess several zero-spin-current points with the increase of temperature. The nonmagnetic achiral nanotubes with SOC have potential device applications in thermal-spin multi-switcher. Moreover, strain engineering in the radical direction of achiral nanotubes is an effective way to improve and control the SSE. It should be pointed out that these unique thermal spin transport phenomena induced by SOC have not been found in the SSE based on conduction electrons in magnetic materials. These theoretical results will enrich the SSE science and expand device applications. Meanwhile, two separate research fields, i.e., spin orbitronics and spin caloritronics, may converge together to a new research subject: spin-orbito-caloritronics.

ACKNOWLEDGMENTS

This work is supported by the National Natural Science Foundation of China with grant No. 11774104 and 11274128. Work at UCI was supported by DOE-BES (Grant No. DE-FG02-05ER46237). Computer simulations were partially performed at the U.S. Department of Energy Supercomputer Facility (NERSC).

* hhfu@mail.hust.edu.cn
† wur@uci.edu

[1] G. E. W. Bauer, E. Saitoh, and B. J. van Wees, Spin caloritronics, Nat. Mater. **11**, 391 (2012).
[2] S. R. Boona, R. C. Myers, and J. P. Heremans, Spin caloritronics, Energy Environ. Sci. **7**, 885 (2014).
[3] K. Uchida, S. Takahashi, K. Harii, J. Ieda, W. Koshibae, K. Ando, S. Maekawa, and E. Saitoh, Observation of the spin Seebeck effect, Nature **445**, 778 (2008).
[4] T. Kikkawa, K. Uchida, Y. Shiomi, Z. Qiu, D. Hou, D. Tian, H. Nakayama, X. F. Jin, and E. Saitoh, Longitudinal spin Seebeck effect free from the proximity Nernst effect, Phys. Rev. Lett. **110**, 067207 (2013).
[5] K. Uchida, J. Xiao, H. Adachi, J. Ohe, S. Takahashi, J. Ieda, T. Ota, Y. Kajiwara, H. Umezawa, H. Kawai, G. E. W. Bauer, S. Maekawa, and E. Saitoh, Spin Seebeck insulator, Nat. Mater. **9**, 894 (2010).
[6] G. Tang, X. Chen, J. Ren, and J. Wang, Recfifying full-counting statistics in a spin Seebeck engine, Phys. Rev. B **97**, 081407 (2018).
[7] Y. Kajiwara, K. Harii, S. Takahashi, J. Ohe, K. Uchida, M. Mizuguchi, H. Umezawa, H. Kawai, K. Ando, K. Takanashi, S. Maekawa, and E. Saitoh, Transmission of electrical signals by spin-wave interconversion in a magnetic insulator, Nature **464**, 262 (2010).
[8] L. J. Cornelissen, J. Liu, R. A. Duine, J. B. Youssef, and B. J. van Wees, Long-distance transport of magnon spin information in a magnetic insulator at room temperature, Nat. Phys. **11**, 1022 (2015).
[9] M. Matsuo, Y. Ohnuma, T. Kato, and S. Maekawa, Spin current noise of the spin Seebeck effect and spin pumping, Phys. Rev. Lett. **120**, 037201 (2018).
[10] L. Gu, H.-H. Fu, and R. Wu, How to control spin-Seebeck current in a metal-quantum dot-magnetic insulator junction, Phys. Rev. B **94**, 115433 (2016).
[11] M. Zeng, Y. Feng, and G. Liang, Graphene-based spin caloritronics, Nano. Lett. **11**, 1369 (2011).
[12] K. Zberecki, M. Wierzbicki, J. Barnaś, and R. Swirkowicz, Thermoelectric effects in silicene nanoribbons, Phys. Rev. B **88**, 115404 (2013).
[13] H.-H. Fu, D.-D. Wu, L. Gu, M. Wu, and R. Wu, Design for a spin-Seebeck diode based on two-dimensional materials, Phys. Rev. B **92**, 045418 (2015).
[14] K. Zberecki, R. Swirkowicz, and J. Barnaś, Spin effects in thermoelectric properties of Al- and P-doped zigzag silicene nanoribbons, Phys. Rev. B **89**, 165419 (2014).
[15] J. Li, B. Wang, F. Xu, Y. Wei, and J. Wang, Spin-dependent Seebeck effects in graphene-based molecular junctions, Phys. Rev. B **93**, 195426 (2016).
[16] D. Hirobe, M. Sato, T. Kawamata, Y. Shiomi, K.-I. Uchida, R. Iguchi, Y. Koike, S. Maekawa, and E. Saitoh, One-dimensional spinon spin currents, Nat. Phys. **13**, 30 (2016).
[17] D.-D. Wu, H.-H. Fu, Q.-B. Liu, G.-F. Du, and R. Wu, Magnetic nanotubes: a new material platform to realize a robust spin-Seebeck effect and a perfect thermal spin-filtering effect. Phys. Rev. B **98**, 115422 (2018).
[18] B. Göhler, V. Hamelbeck, T. Z. Markus, M. Kettner, G. F. Hanne, Z. Vager, R. Naaman, and H. Zacharias, Spin selectivity in electron transmission through self-assembled monolayers of double-stranded NDA. Science **331**, 894-897 (2011).
[19] T. J. Zwang, S. Hürlimann, M. G. Hill, and J. K. Barton, Helix-dependent spin filtering through the DNA duplex. J. Am. Chem. Soc. **138**, 15551-15554 (2016).
[20] C. Fontanesi, Spin-dependent electrochemistry: a novel paradigm, Curr. Opin. Elect. **7**, 36-41 (2018).
[21] R. Naaman and D. H. Waldeck, Chiral-induced spin selectivey effect, J. Phys. Chem. Lett. **3**, 2178-2187 (2012).
[22] V. Kiran, S. P. Mathew, S. R. Cohen, I. H. Delgado, J. Lacour,and R. Naaman, Helicenes - a new class of organic spin filter, Adv. Mater. **28**, 1957 (2016).
[23] J. Vacek, J. V. Chocholoušová, I. G. Stará, I. Starý, and Y. Dubi, Mechanical tuning of conductance and thermopower in helicene molecular jucntions, Nanoscale **7**, 8793 (2015).

[24] A.-M. Guo and Q.-F. Sun, Spin-Selective transport of electrons in DNA double helix, Phys. Rev. Lett. **108**, 218102 (2012).

[25] A.-M. Guo and Q.-F. Sun, Sequence-dependent spin-selective tunneling along double-stranded DNA, Phys. Rev. B **86**, 115441 (2012).

[26] T.-R. Pan, A.-M. Guo, and Q.-F. Sun, Spin-polarized electron transport through helicene molecular junctions, Phys. Rev. B **94**, 235448 (2016).

[27] A.-M. Guo, T.-R. Pan, T.-F. Fang, X.-C. Xie, and Q.-F. Sun, Spin selectivety effect in achiral molecular systems, Phys. Rev. B **94**, 165409 (2016).

[28] S. Varela, V. Mujica, and E. Medina, Effective spin-orbit couplings in an analytical tight-binding model of DNA: Spin filtering and chiral spin transport, Phys. Rev. B **93**, 155436 (2016).

[29] T. Kuschel and G. Reiss, Spin orbitronics charges ride the spin wave, Nat. Nanotech. **10**, 22-24 (2015).

[30] M. Kepenekian and J. Even, Rashba and Dresselhaus couplings in Halide Perovskites: accomplishments and opportunities for spintronics and spin-orbitronics, J. Phys. Chem. Lett. **8**, 3362-3370 (2017).

[31] A.-M. Guo and Q.-F. Sun, Spin-dependent electron transport in protein-like single-helical molecules, Pro. Natl. Acade. Sci. USA **111**, 11658-11662 (2014).

[32] Y. Xiang, Q.-F. Sun, and J. Wang, Influence of dephasing on the quantum Hall effect and the spin Hall effect, Phys. Rev. B **77**, 115346 (2008).

[33] Y. Imry and R. Laudaüer, Conductiance viewed as transission, Rev. Mod. Phys. **71**, S306 (1999).

[34] S. Datta, Electronic Transport in Mesoscopic Systems (Cambridge University Press, Cambridge, 1995).

[35] D.-D. Wu, Q.-B. Liu, H.-H. Fu, and R. Wu, How to realize a spin-dependent Seebeck diode effect in metallic zigzag gammagraphyne nanoribbons? Nanoscale **9**, 18334 (2017).

[36] H.-H. Fu, and K.-L. Yao, Spin-filter and Fano antiresonant effect in conductance through a zigzaglike polymer device: nonequilibrium Green's function approach, J. Chem. Phys. **134**, 054903 (2011).

[37] H.-H. Fu, and K.-L. Yao, Perfect spin-filter and highly spin-polarized current in a quantum network device, Appl. Phys. Lett. **100**, 013502 (2012).

[38] M. Shirdel-Havar and R. Farghadam, Spin caloritronics in spin semiconducting armchair graphene nanoribbons, Phys. Rev. B **97**, 235421 (2018).

[39] B.-L. Li and K.-Q. Chen, Effects of electron-phonon interactions on the spin-dependent Seebeck effect in graphene nanoribbons, Carbon **119**, 548-554 (2017).

[40] D.-D. Wu, H.-H. Fu, Q.-B. Liu, and R. Wu, How to realize the spin-Seebeck effect with a high spin figure of merit in magnetic boron-nitrogen nanoribbon and nanotube structures? J. Mater. Chem. C. **6**, 10603-10610 (2018).

[41] J. Li, B. Wang, F. Xu, Y. Wei, and J. Wang, Spin-dependent Seebeck effects in graphene-based molecular junctions, Phys. Rev. B **93**, 195426 (2016).

[42] Z.-Q. Zhang, Y.-R. Yang, H.-H. Fu, and R. Wu, Design of spin-Seebeck diode with spin semiconductors, Nanotechnology **27**, 505201 (2016).

[43] R. Hafizi, J. Tersoff, and W. Perebeinos, Band Structure and Contact Resistance of Carbon Nanotubes Deformed by a Metal Contact, Phys. Rev. Lett. **119**, 207701 (2017).

[44] B. Huang, K.-H. Jin, B. Cui, F. Zhai, J. Mei, and F. Liu, Bending strain engineering in quantum spin hall system for controlling spin currents, Nat. Commun. **8**, 15850 (2017).

[45] M.-F. Yu, O. Lourie, M. J. Dyer, K. Moloni, T. F. Kelly, and R. S. Ruoff, Strength and breaking mechanism of multiwalled carbon nanotubes under tensile load, Science **287**, 637 (2000).

[46] I. Palaci, S. Fedrigo, H. Brune, C. Klinke, M. Chen, and E. Riedo, Radial elasticity of multiwalled carbon nanotubes, Phys. Rev. Lett. **94**, 175502 (2005).

[47] M.-F. Yu, T. Kowalewski, and R. S. Ruoff, Investigation of the radial deformability of individual carbon nanotubes under controlled indentation force, Phys. Rev. Lett. **85**, 1456 (2000).

[48] See Supplemental Material at http://link.aps.org /supplemental/$***$ for details.